1. GENERAL FEATURES

FIGURE 1.1.—Lunar nearside photographed 4 days after full Moon from the Pic du Midi Observatory, France, in August 1964. Left (west) half is illuminated at high Sun elevations, which enhance albedo (brightness) variations, and right (east) part at lower Sun elevations, which enhance relief by casting shadows. Terminator (line between dark and illuminated areas) is at long 51° E. Extensive ray systems surround craters Copernicus (upper left center) and Tycho (near bottom). Mare Nectaris, surrounded by concentric rings, is along terminator at lower right.

Note: Before 1961, lunar directions were stated with reference to their position in the sky as viewed from the Earth. Mare Orientale, the "Eastern Sea," is on the left limb of the Moon as seen in the Northern Hemisphere, that is, near the east horizon of the Earth. In 1961, the "astronautical convention" was adopted in anticipation of manned spaceflight: The direction from which the Sun rises on the Moon was henceforth called east, as it is on the Earth. The definition of north remained the same, but after 1961, more publications began orienting their figures with north at the top rather than at the bottom (as it is seen in astronomic telescopes). The 0° meridian is in the center of the nearside, and the diametrically opposite longitudal line on the farside is 180°. On most maps, longitudes increase both eastward and westward from the 0° meridian until meeting at the 180° meridian, which is also the terrestrial convention. Some lunar maps use a 360° system of longitudes, increasing eastward from the 0° central meridian. In this volume, the Orientale limb is considered the west, photographs are oriented with north at the top except as noted, nearside longitudes are less than 90°, and farside longitudes are greater than 90°.

1. GENERAL FEATURES

CONTENTS

SURFACE

Near full Moon, the naked eye sees a contrast between dark and light surfaces (of low and high *albedo*, respectively) that has been fancied as a "man in the Moon" or other configurations (fig. 1.1). In 1609, Galileo noted that the dark spots are smooth and the brighter areas rugged (Whitaker, 1978). These terrain types are still designated by their 17th-century names *maria* (singular, *mare*) and *terrae* (singular, *terra*; commonly known as uplands or highlands; table 1.1). The maria constitute about 16 percent, and the terrae 84 percent, of the lunar surface. Maria occupy about 30 percent of the lunar *nearside*, the hemisphere visible from the Earth; spacecraft exploration, beginning with the Soviet Luna 3 in 1959 (table 1.2; Barabashov and others, 1961; Kopal and Mikhailov, 1962, p. 1–44; Whitaker, 1963), showed that they constitute only about 2 percent of the *farside* (figs. 1.2–1.4). South of about lat 35° S., however, the proportions are reversed; the southern farside is richer in maria than is the southern nearside (fig. 1.5).

Most of the maria are approximately circular. The circular maria are bordered by annular or arcuate, commonly mountainous terra rims. The terra structures in which the circular maria lie are called *ringed basins* or, simply, *basins* (see chap. 4; table 1.1; Hartmann and Kuiper, 1962). Most large mountainous rings or arcs that do not encompass maria are also parts of basins (figs. 1.4, 1.5). Concentric rings characterize all well-exposed basins.

TABLE 1.1.—*Names of common lunar landforms*

[Plural form in parentheses; the singular form is properly used adjectivally--for example, "mare basalt" rather than "maria basalt."]

[Latin generic terms and proper names of individual features used here are approved by the International Astronomical Union (Arthur and others, 1963; Andersson and Whitaker, 1982). Small or obscure craters have traditionally been designated by letters after the names of a nearby, more conspicuous crater (Mädler system of nomenclature); following Andersson and Whitaker, these convenient lettered names are used in this volume in preference to some new names that were invented for use on the large-scale charts made from Apollo orbital data]

Latin name	Common name	Description
Mare (maria)	Sea (not used in this volume).	Dark, smooth plains.
Lacus, palus, sinus		Small mare.
Terra (terrae)[1]	Highlands, uplands, continents.	Rugged, relatively bright (high albedo) terrain.
Mons (montes)	Mount, mountain(s)	High massif(s), generally forming arcuate ranges.
Promontorium	Promontory	Mountains partly enclosed by mare.
Rupes	Scarp	Fault in mare or high arcuate scarp in terra.
Dorsum (dorsa)	Mare ridge, wrinkle ridge.	Narrow ridge, mostly in mare.
Rima (rimae)	Rille	Narrow, elongate depression (sinuous, arcuate, or straight).
Vallis (valles)	Valley	Wide, elongate depression, commonly consisting of inconspicuous craters.
Catena (catenae)	Chain	Chain of distinct craters.
	Crater	Circular or subcircular depression, generally bounded by a raised rim.[2]
	Basin, ringed basin	Large craterlike depression containing one or more rings in addition to a rim.[3]

[1]There is no sharp distinction between an individual "terra" and the "terrae." "Terrestrial" refers to the planet Earth.

[2]Usage has established the term "ejecta," for the material thrown out of craters, as a singular noun, despite its origin as a Latin plural.

[3]The terms "mare" and "basin" are commonly confused. Genetically, these two features are only indirectly related (see chap. 2). Basins are terra structures, not all of which contain maria. Efforts to alleviate this serious semantic confusion have led to use of such terms as "mountain-bordered mare," "mare basin," "dry mare," "thalassoid" (no lava; Lipsky, 1965), and "multiringed basin." Terms for basins that contain the word "mare" are unsatisfactory, and even "basin" is misleading because these structures are characterized by huge mountainous rings as much as by the excavated depression. Nevertheless, it is probably too late to coin a new term. In this volume, the term "basin" or "ringed basin" is used for all lunar excavations at least 300 km in diameter; a more exact definition has not yet been agreed upon (see chap. 4).

The maria are mostly level and smooth at coarse scales but contain local topographic relief. *Mare ridges* (*dorsa*) are long intricate welts on the mare surfaces (fig. 1.6). *Rilles* (*rimae*) are narrow troughs or grooves much longer than they are wide; they include genetically distinct sinuous, arcuate, and straight varieties. Few ridges but many arcuate and straight rilles cut the terrae as well as the maria. *Dark-mantling materials* are as dark as or darker than the maria but assume part of the topographic form of the underlying terrain (figs. 1.6, 1.7).

Craters, ranging in size from those visible with binoculars to micropits observed on returned samples, are ubiquitous on the lunar surface. At coarse scales, they are much more numerous on the terrae than on the maria. Most lunar craters have rims elevated above, and floors depressed below, the surrounding terrain. Craters smaller than about 16 to 21 km in diameter have relatively featureless interiors; larger craters are more complex, possessing central peaks, arcuate wall terraces, and other interior landforms (see chap. 3). Some crater exteriors resemble the adjacent terrain except for a short rim flank; others display coarse concentric structure near the rim crest, grooves on a lower rim flank, and numerous smaller *satellitic craters*, which are most conspicuous between about one and three crater radii from the rim (fig. 1.6). Bright *rays* radiate hundreds or thousands of kilometers from some craters (figs. 1.1, 1.6).

Most terrae appear at first glance to consist of little except large, randomly distributed, overlapping craters. However, regional differences in terra morphology emerge upon further inspection (Hackman and Mason, 1961). The central and northern nearside is characterized by ridges and grooves radial to the Imbrium basin, which contains Mare Imbrium (figs. 1.6–1.8). The terra east of the neighboring circular basin, Serenitatis, has a choppier, less regular pattern of elevations and depressions (fig. 1.7). Several regions contain particularly dense concentrations of craters that are grouped in chains or clusters. Concentric arcs of the Nectaris basin, which encompass the small Mare Nectaris, are conspicuous in the southeast quadrant (fig. 1.1). An even more conspicuous system of concentric rings, radial lineations, and satellitic craters surrounds Mare Orientale on the west limb of the Moon (fig. 1.9). *Terra plains* that are smooth and level like the maria, but lighter in color, occupy more crater floors and other depressions in and near the Imbrium- and Orientale-radial terrains (figs. 1.8, 1.9) than in any other region. These textural patterns in the Imbrium, Nectaris, and Orientale regions, as described in detail in this volume, play major roles in elucidating the geology of the Moon. They are expressions of major stratigraphic units and form the basis for interpreting less distinctive terrae.

The farside seems, at first, to be even less regularly patterned than the nearside. This difference is due mostly to the absence of maria and of the extensive circum-Imbrium radial pattern that characterize the nearside terrae. Later descriptions show that concentric and radial patterns also characterize the farside (fig. 1.4), although they are generally less extensive, less pronounced, and less well photographed than those of the nearside. The southern farside, which contains most of the farside's maria, also contains the farside's most conspicuous concentric rings and other noncrater morphologies (fig. 1.5). A major purpose of this volume is to show the basic stratigraphic order that underlies the morphologic features of the terrae.

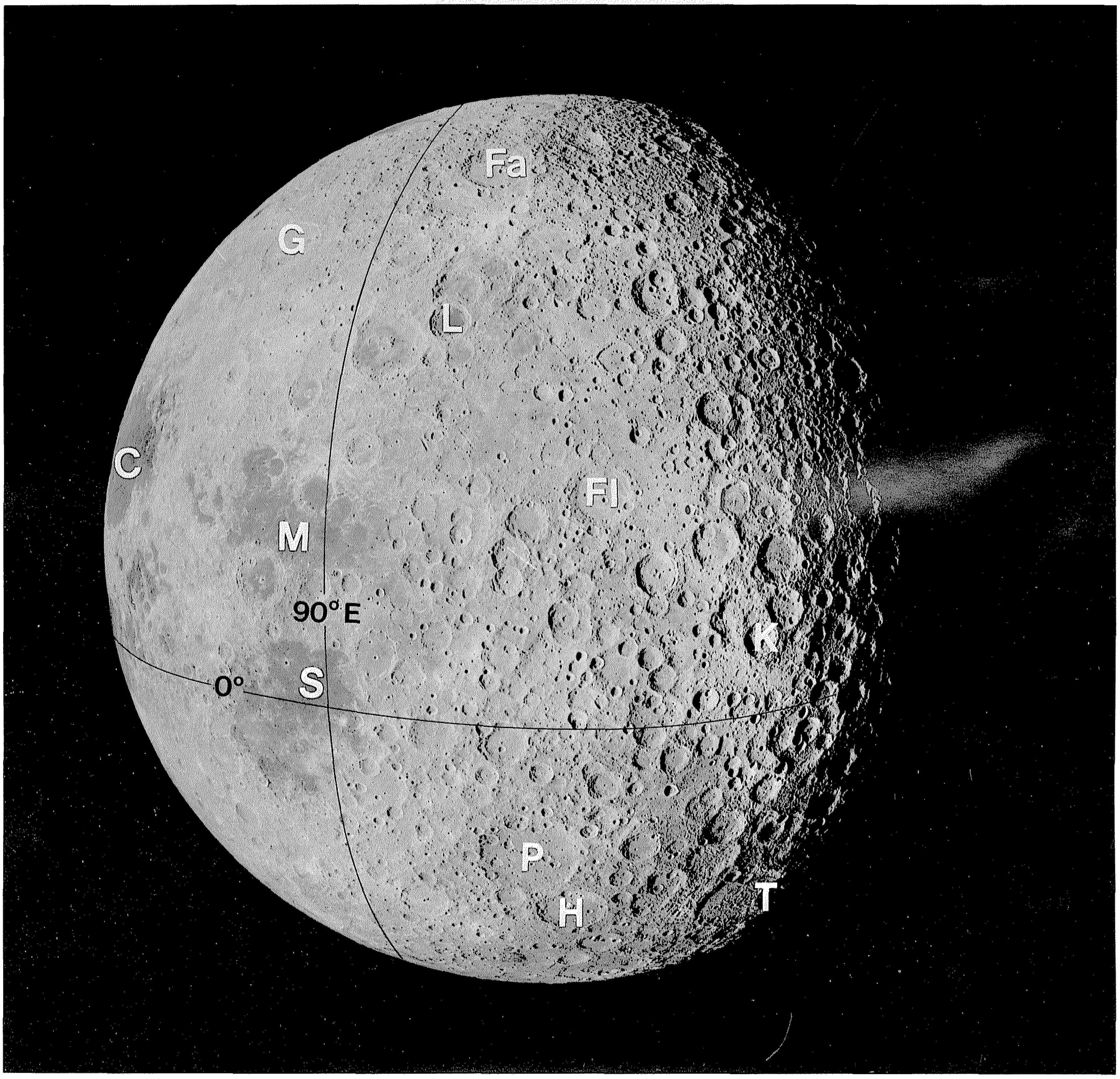

FIGURE 1.2.—East limb (right edge of lunar disc as seen from the Earth) and adjacent part of farside, divided by long 90° E. Mare Crisium (C) is on nearside, and Maria Marginis (M) and Smythii (S) partly on farside. Maria also fill such craters as Lomonosov (L; 93 km, 27° N., 98° E.) and Tsiolkovskiy (T; 180 km, 20° S., 129° E.; partly in shadow; compare figs. 1.3, 1.4). Farside terrane in view, which is otherwise mostly terra, includes craters Fabry (Fa; 179 km, 43° N., 101° E.), Fleming (Fl; 130 km), Hilbert (H; 170 km), King (K; 77 km), and Pasteur (P; 235 km). A large subcircular area of light-colored plains lies between Fleming and Lomonosov. Terminator is at long 131° E.; left-hand (west) edge of photograph is at nearly the same longitude as terminator in figure 1.1. Apollo 16 frame M–3021, photographed by Apollo 16 mapping camera on Earthbound flight in April 1972.

Note: This volume includes photographs taken with three types of cameras carried in lunar orbit by Apollo spacecraft: mapping or metric (M), panoramic (P), and hand-held or bracket-mounted Hasselblads (H). All missions carried Hasselblads; Apollos 15 through 17 carried both mapping and panoramic cameras as well (pl. 2; Masursky and others, 1978).

Note: Most crater diameters and positions in this volume are from Andersson and Whitaker (1982). Basin diameters and most crater diameters used in frequency studies are from my measurements. Latitude is given before longitude throughout the volume. Coordinates differ considerably among various maps, especially on the limbs and farside. One degree of lunar latitude covers about 30 km.

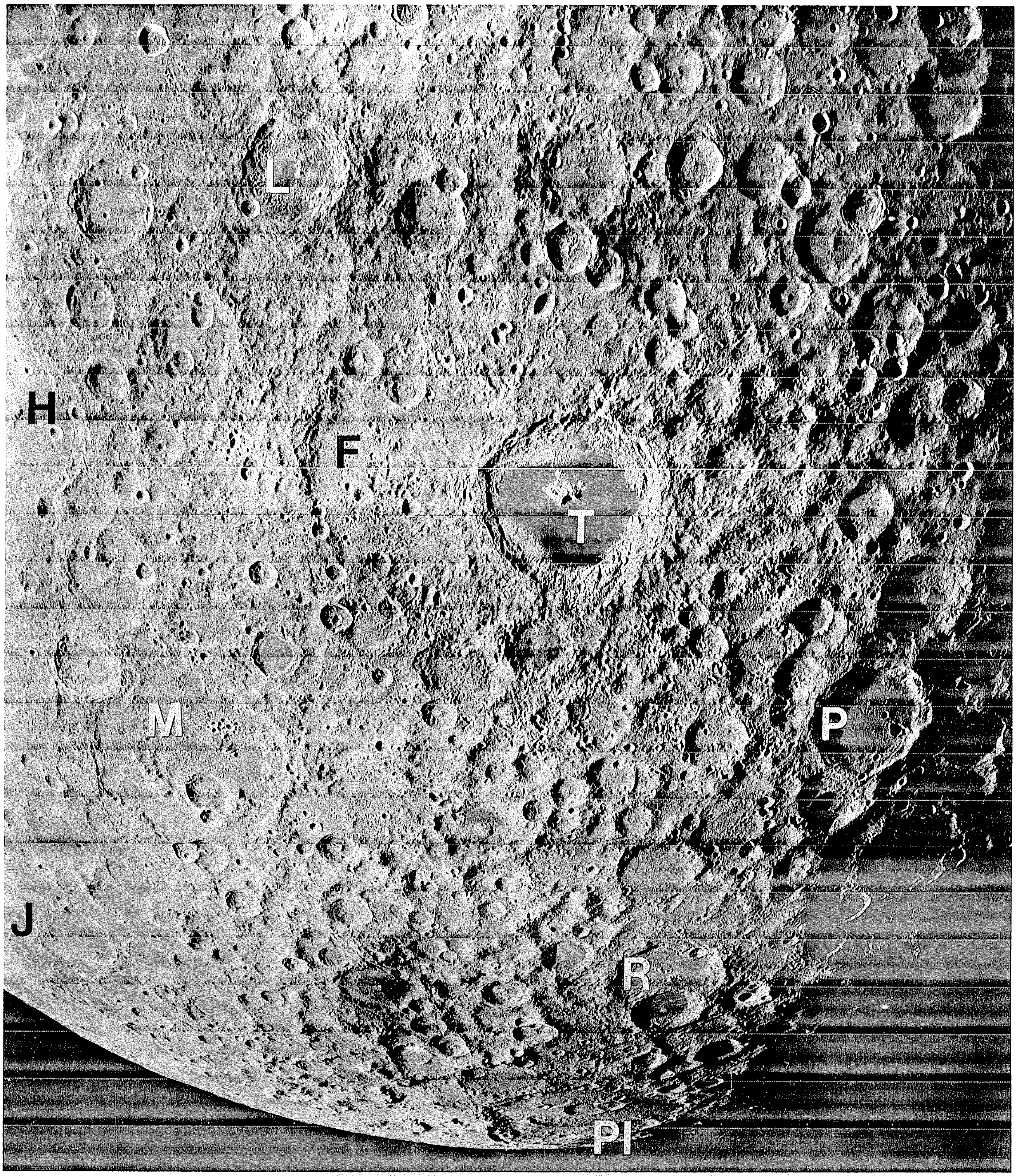

FIGURE 1.3.—Part of southern farside centered on mare-filled crater Tsiolkovskiy (T). Overlaps with fig. 1.2; compare Tsiolkovskiy and Hilbert (H; 170 km, 18° S., 108° E.). Other craters: Langemak (L; 102 km; contains small mare patch), Fermi (F; 238 km), Milne (M; 262 km; fig. 1.5), Jenner (J; 72 km; fig. 1.5), Pavlov (P; 141 km), Roche (R; 146 km; superposed crater Pauli contains mare). Pl, small ringed basin Planck (325 km, 60° S., 136° E.; figs. 1.4, 1.5). Orbiter 3 frame M–121.

Note: Photographs transmitted from unmanned Lunar Orbiter spacecraft in 1966 and 1967 (table 1.2; Levin and others, 1968; Mutch, 1970) are labeled as follows: "Orbiter" followed by mission number (1–5), M (medium resolution) or H (high resolution), and frame number. Best Lunar Orbiter coverage of each area is outlined on plate 2.

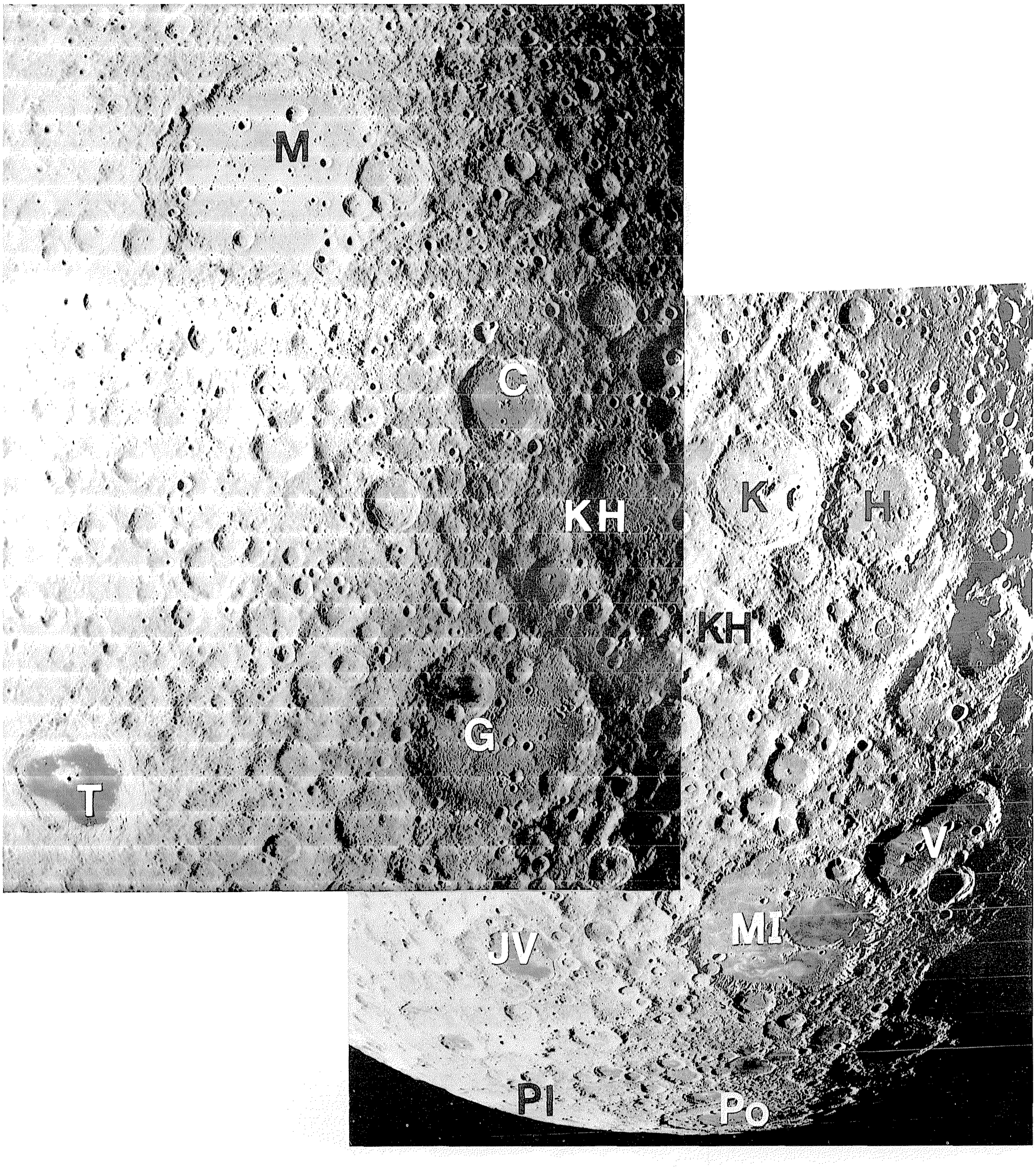

FIGURE 1.4.—Equatorial and southern farside. Most of area is heavily cratered, smoother in Gagarin (G; 272 km, 20° S., 149° E.) and north of Heaviside (H; 163 km, 11° S., 167° E.). A distinct linear trough is north of Keeler (K; 169 km). Arcuate massifs below and to left (west) of Keeler and Heaviside are parts of Keeler-Heaviside basin (KH). Maria fill Tsiolkovskiy (T), Mare Ingenii (MI, in Ingenii basin), Jules Verne (JV; 134 km), part of Poincaré basin (Po; compare fig. 1.5), and other depressions. Other craters: Chaplygin (C; 124 km) and Van de Graaff (V, double); other basins: Planck (Pl, compare fig. 1.3) and Mendeleev (M; 320 km, 6° N., 142° E.). Mosaic of Orbiter 1 frame M–115 (left) and Orbiter 2 frame M–75 (right).

FIGURE 1.5.—Southeast limb, showing concentration of maria and various ringed basins (see chap. 4). A, massifs of Australe basin, which enclose Mare Australe, consisting of many small mare matches resting in such craters as Jenner (J; compare fig. 1.3) and Lyot (L; 141 km); An, Antoniadi crater or basin (135 km); C, outer ring of Crisium basin; M, Milne (compare fig. 1.3); MS, Mare Smythii in Smythii basin (compare fig. 1.2); Pl, Planck basin (barely discernible; compare fig. 1.3); Po, Poincaré basin, containing several mare patches (compare fig. 1.4); S, Schrödinger double-ringed basin (320 km, 76° S., 134° E.). Indefinite basins (table 4.2) include Amundsen-Ganswindt (AG), Balmer-Kapteyn (BK), and Sikorsky-Rittenhouse (SR). Grooves are radial to Schrödinger and to Nectaris basin (N; basin is outside photograph). Crater Humboldt (H; 207 km, 27° S., 81° E.) contains rilles and small mare patches. Orbiter 4 frame M–9.

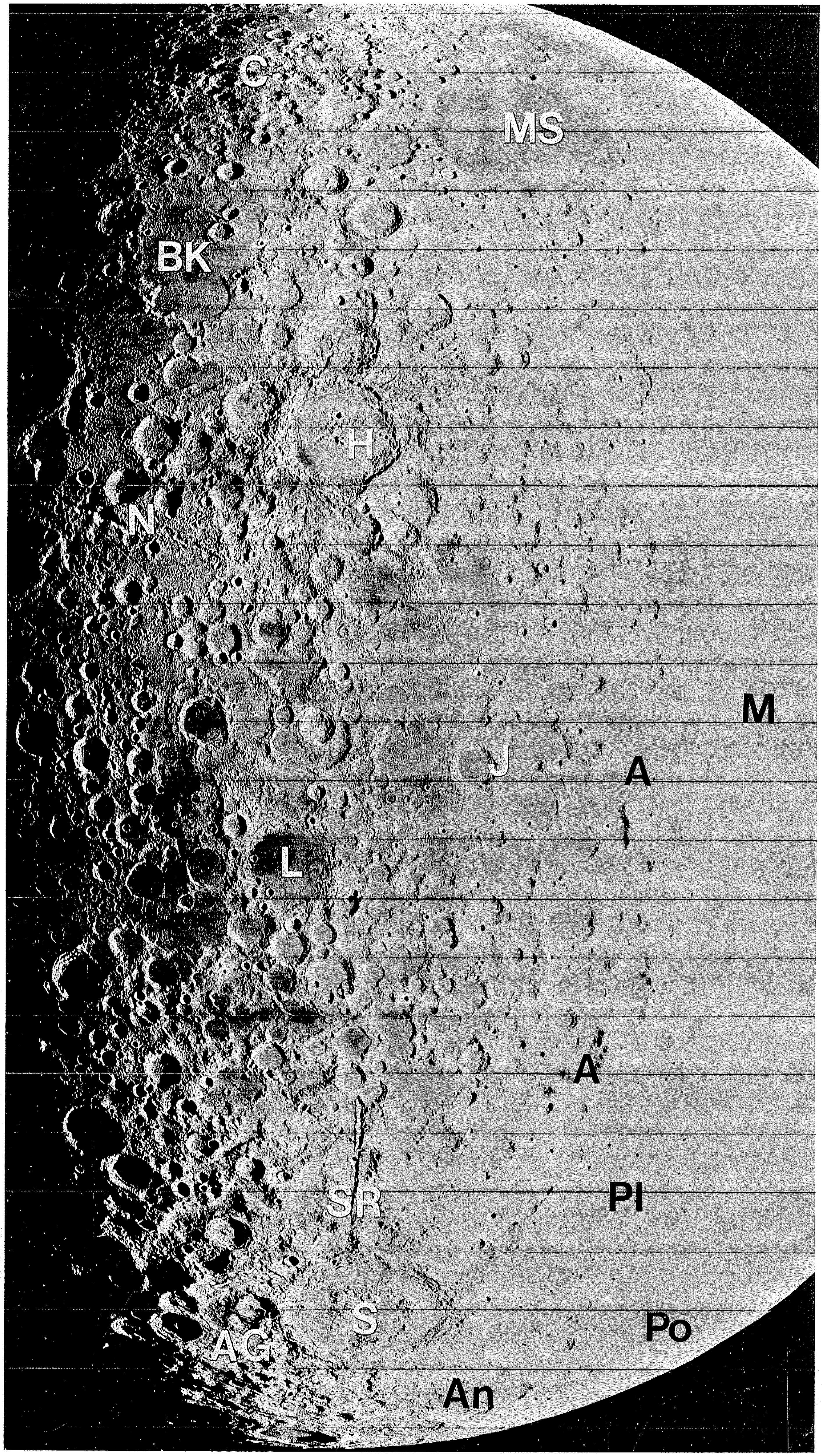

C
MS
BK
H
N
M
J
A
L
A
SR
Pl
S
Po
AG
An

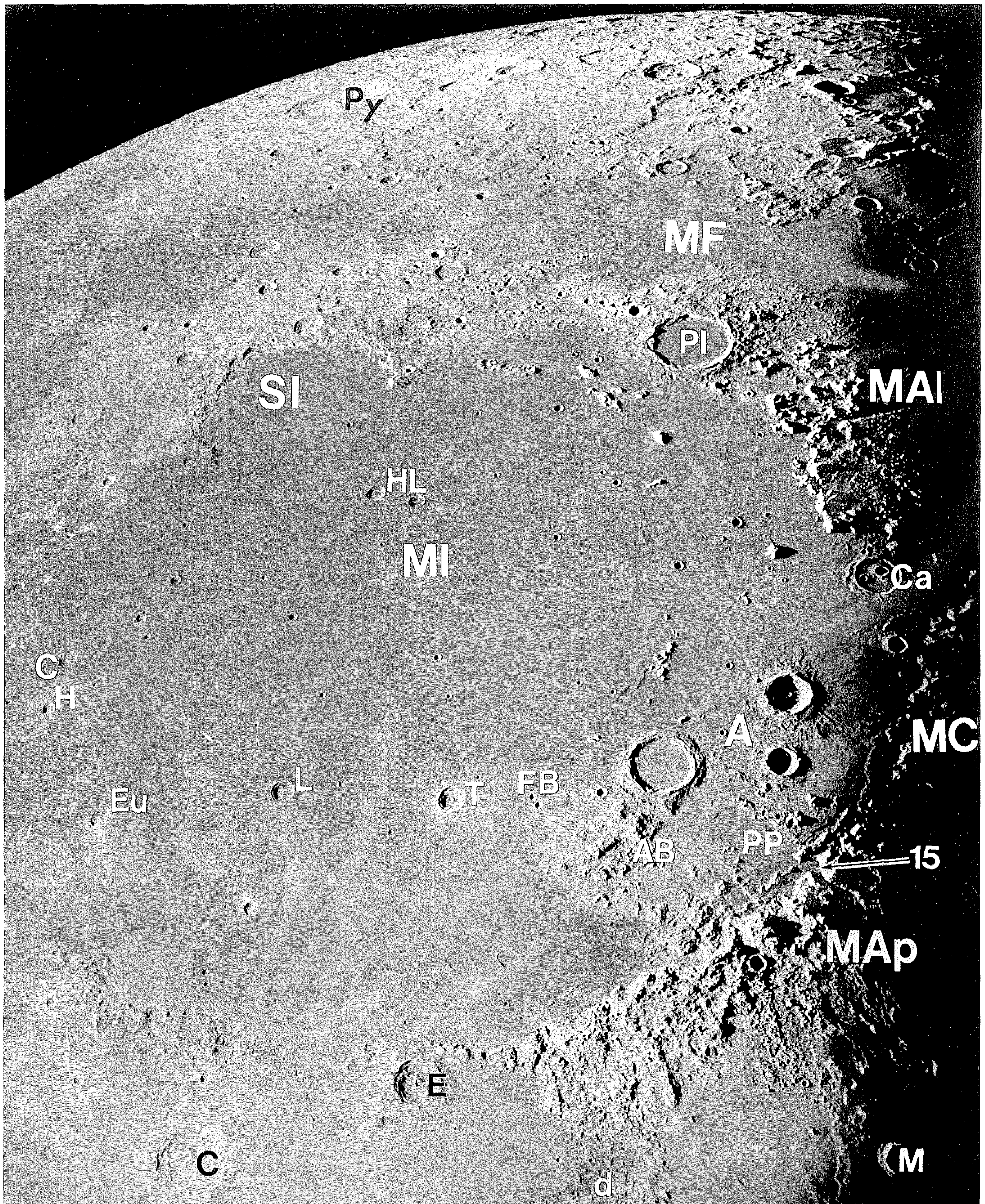

FIGURE 1.6.—Telescopic view of circular Mare Imbrium (MI) and Imbrium basin. MF, Mare Frigoris; PP, Palus Putredinis; arrow, Apollo 15 landing site. Imbrium-basin rim is composed of Montes Alpes (MAl), Montes Apenninus (MAp), Montes Caucasus (MC), and terra occupied by Iridum crater bounding mare feature Sinus Iridum (SI). Lunar stratigraphic scheme of Shoemaker and Hackman (1962) is based on relations among Imbrium basin, planar material of Apennine Bench (AB), Archimedes (left of A), mare material, Eratosthenes (E), and Copernicus (C; 95 km; compare fig. 1.1; satellitic craters are visible east of crater) (see chaps. 2, 7). "Wrinkle ridges" (dorsa) are above A; rilles are below PP. Crater pairs (see chap. 3) include Aristillus and Autolycus (right of A), Caroline Herschel and Heis (CH), Feuillée and Beer (FB), and Helicon and Leverrier (HL). Other features: Cassini (Ca), Euler (Eu), Lambert (L), Manilius (M), Plato (Pl), Pythagoras (Py), and Timocharis (T); many irregular craters north of Mare Frigoris; d, dark-mantled terra surface. Mount Wilson Observatory photograph, catalog No. 257.

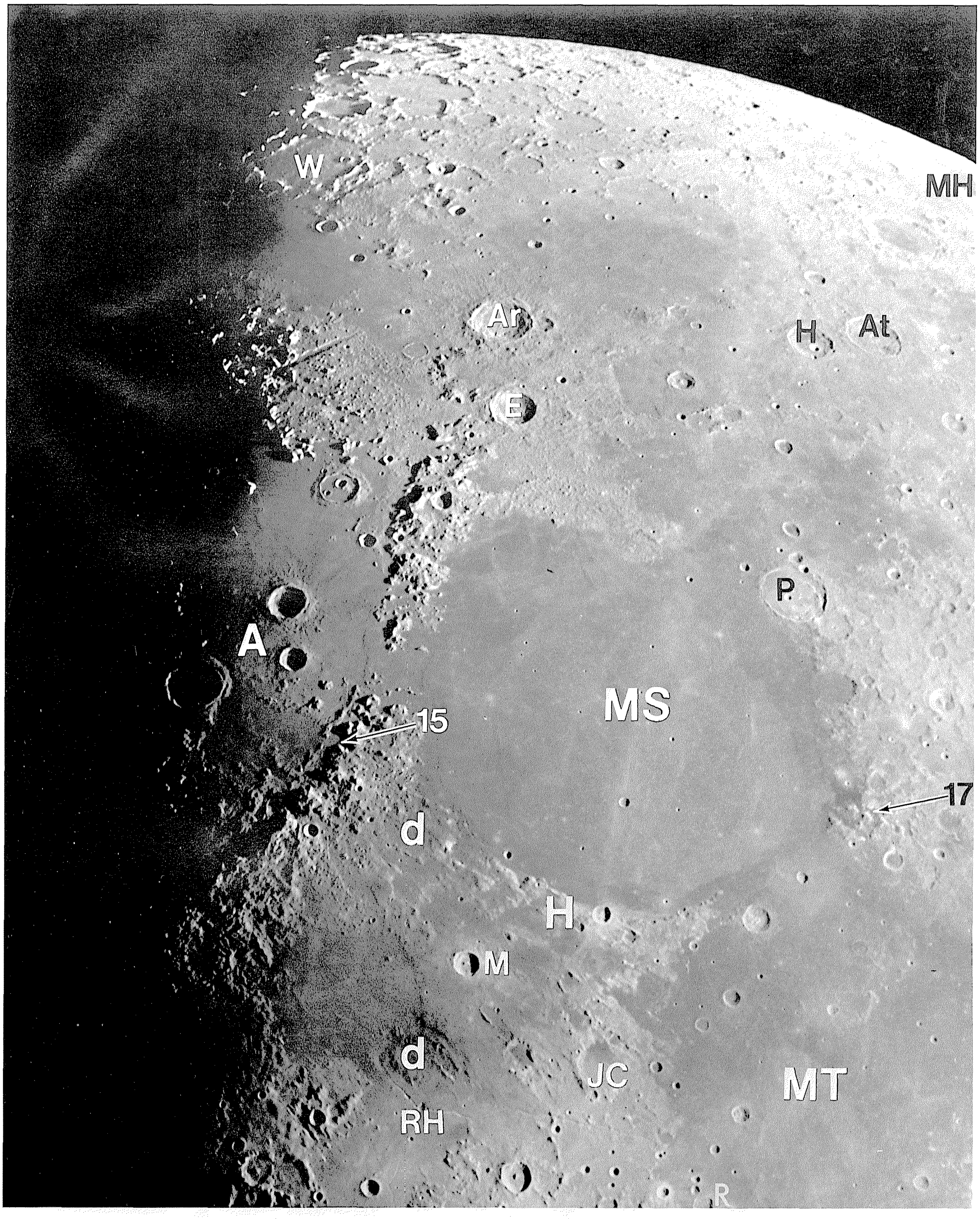

FIGURE 1.7.—Telescopic view centered on Mare Serenitatis (MS), overlapping area of figure 1.6. Lineations in Montes Haemus (H) on southern part of Serenitatis rim are radial to Montes Apenninus; nonlineate hummocky terrain adjoins Montes Caucasus and Montes Alpes. Terrain east of Mare Serenitatis consists of irregular craters and massifs. Other features: Ar, Aristoteles (87 km, 50° N., 17° E.); At, Atlas (87 km); E, Eudoxus; H, Hercules; JC, Julius Caesar; M, Manilius; MH, Mare Humboldtinaum; MT, Mare Tranquillitatis; P, Posidonius; R, Ritter (29 km, 2° N., 19° E.); RH, Rima Hyginus; densely cratered northern terrain including W. Bond (W; 158 km, 65° N., 4° E.); d, dark-mantling material. Arrows, Apollo 15 and 17 landing sites. Mount Wilson Observatory photograph, catalog No. 262.

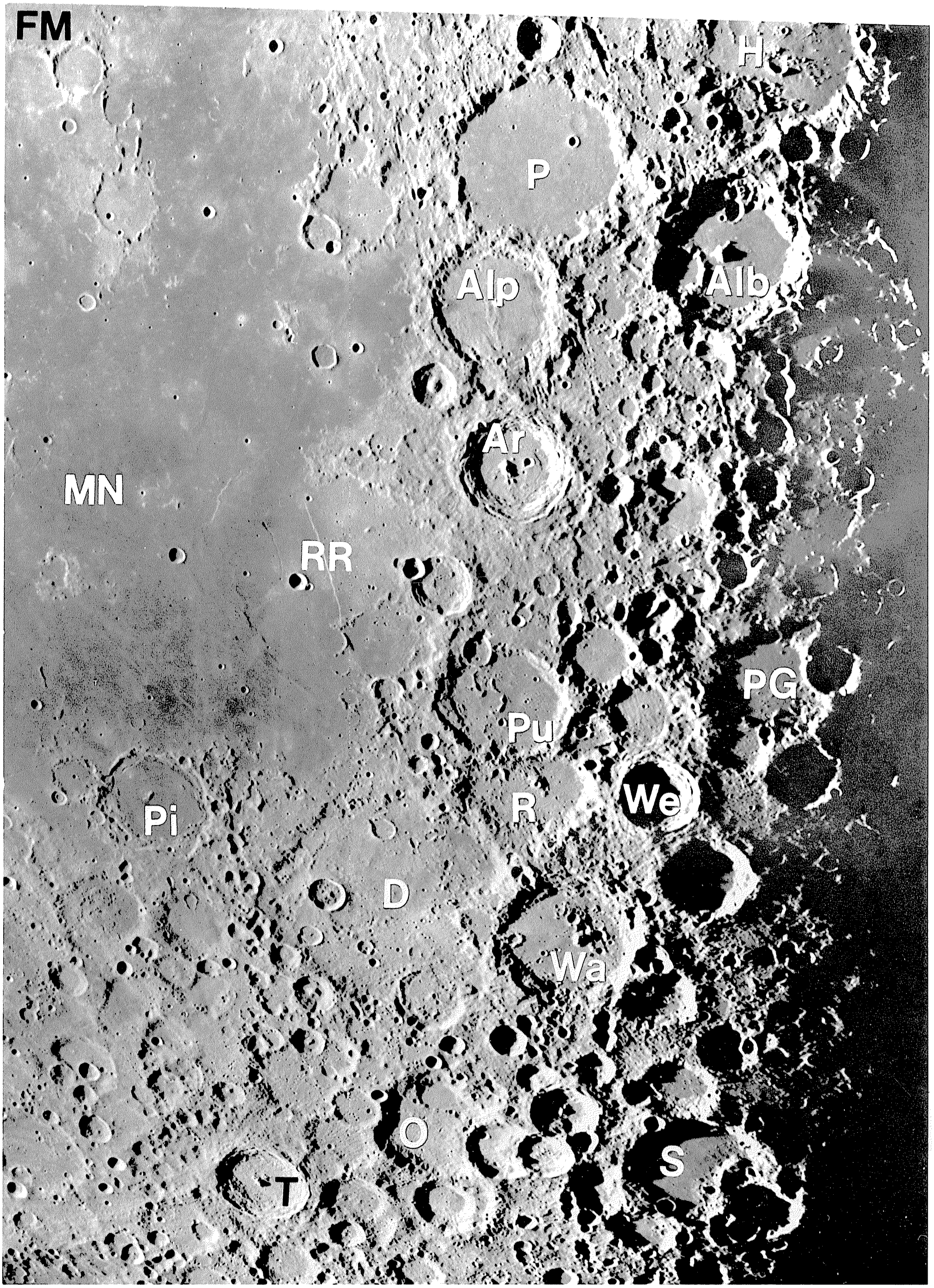
FM
H
P
Alp
Alb
Ar
MN
RR
PG
Pu
We
R
Pi
D
Wa
O
S
T

FIGURE 1.9.—Southwest limb (lower left as seen from northern hemisphere of the Earth). Arrows indicate long 90 W.; upper arrow on equator and lower on south pole. Conspicuous lineations are radial to Mare Orientale and ringed Orientale basin (centered at 20° S., 95° W.). Light-colored plains form part of terrain outside Orientale radials, for example, in Schiller-Zucchius basin (SZ), in central part of crater Schickard (S; 227 km, 44° S., 55° W.), and in and near crater Wargentin (W; 84 km). Other basins: Bailly (B; 300 km, 67° S., 69° W.), Grimaldi (G; partly mare-filled), Mendel-Rydberg (MR, barely visible), and South Pole-Aitken (SA, mountainous massifs); OP, part of Oceanus Procellarum in Procellarum basin. Footprint-shaped crater is Schiller (180 km). Orbiter 4 frame M–180.

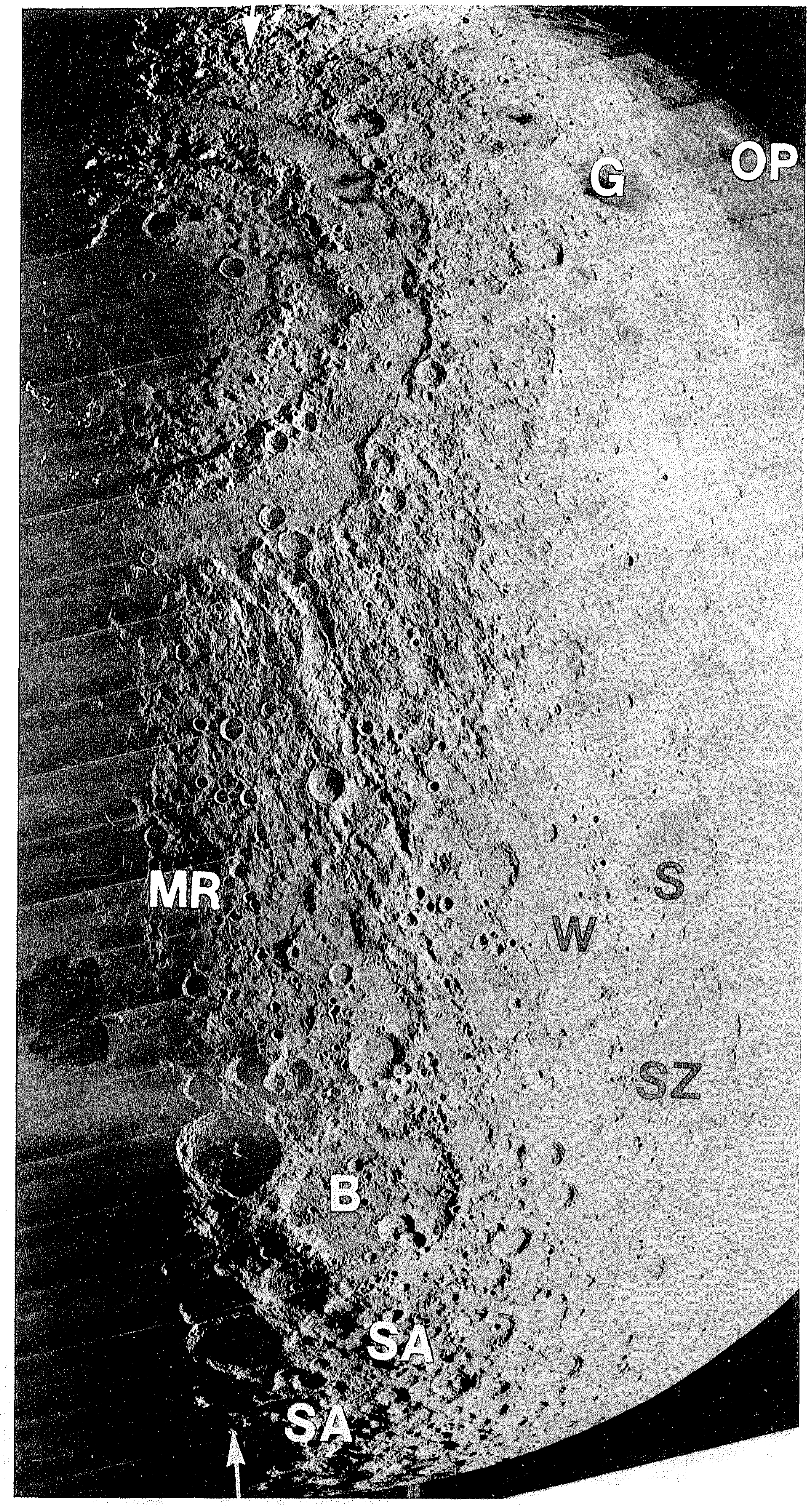

FIGURE 1.8.—South-central nearside, including parts of "Fra Mauro peninsula" (FM) and Mare Nubium (MN), mare-filled crater Pitatus (Pi), fresh crater Tycho (T; 85 km, 43° S., 11° W.; compare fig. 1.1), moderately fresh crater Werner (We), and north-south-trending "backbone" of terra, including "chain" of large craters Ptolemaeus (P; 153 km, 9° S., 2° W.), Alphonsus (Alp), Arzachel (Ar), Purbach (Pu), Regiomontanus (R), and Walter (Wa, 140 km, 33 S., 1° E). Smooth terra plains lighter than maria fill many craters, including those in "chain" and Albategnius (Alb), Deslandres (D), Hipparchus (H), Orontius (O), Playfair G (PG), and Stöfler (S). Rupes Recta (RR, "Straight Wall") and grooves ("sculpture") in upper right quadrant are radial to Imbrium basin. Apollo 14 landing site is just beyond north edge of photograph, above letters FM. Mount Wilson Observatory photograph.

TABLE 1.2.—*Spaceflights that provided lunar data*

[Dates are beginnings of mission activities at the Moon. Ranger 7 impacted on August 1, 1964 (G.m.t.)]

Mission	Date	Type of mission	Landing location or orbital parameters
Luna 2	Sept. 1959	First impact	Flank of crater Autolycus, lat 30° N., long 0°.
Luna 3	Oct. 1959	First unmanned flyby photography	Farside and east limb; altitude, 65,000 km.
Ranger 7	July 1964	First preimpact photography	Mare Nubium (Cognitum), lat 10.6° S., long 20.7° W.
Ranger 8	Feb. 1965	Preimpact photography	Mare Tranquillitatis, lat. 2.6° N., long 24.7° E.
Ranger 9	Mar. 1965	Last preimpact photography	Floor of crater Alphonsus, lat 12.9° S., long 2.4° W.
Zond 3	July 1965	Unmanned flyby photography	Farside and west limb; altitude, 9,960 to 11,570 km.
Luna 9	Feb. 1966	First unmanned landing	Oceanus Procellarum, lat 7.1° N., long 65.4° W.
Luna 10	Apr. 1966	First unmanned orbital; gamma-ray	Perilune, 350 km.
Surveyor 1	June 1966	Unmanned landing	Mare in crater Flamsteed P, lat 2.5° S., long 43.2° W.
Lunar Orbiter 1	Aug. 1966	First unmanned orbital photography	Inclination, 12°; perilunes, 190 and 40 km.
Luna 11	Aug. 1966	Unmanned orbital photography	Perilune, 165 km.
Luna 12	Oct. 1966	do	Perilune, 100 km.
Lunar Orbiter 2	Nov. 1966	do	Inclination, 12°; perilune, 50 km.
Luna 13	Dec. 1966	Unmanned landing	Oceanus Procellarum, lat 18.9° N., long 62.1° W.
Lunar Orbiter 3	Feb. 1967	Unmanned orbital photography	Inclination, 21°; perilune, 55 km.
Surveyor 3	Apr. 1967	Unmanned landing	Oceanus Procellarum, lat 3.2° S., long 23.4° W.
Lunar Orbiter 4	May 1967	Unmanned orbital photography (global)	Inclination, 85°; perilune, 2,705 km.
Explorer 35	July 1967	Unmanned orbital magnetics	Perilune, 830 km (returned data until Feb. 1972).
Lunar Orbiter 5	Aug. 1967	Unmanned orbital photography	Inclination, 85°; perilunes, 195 and 100 km.
Surveyor 5	Sept. 1967	Unmanned landing, first chemical analysis	Mare Tranquillitatis, lat 1.4° N., long 23.1° E.
Surveyor 6	Nov. 1967	Unmanned landing	Sinus Medii, lat 0.5° N., long 1.5° W.
Surveyor 7	Jan. 1968	First unmanned landing in terra	Flank of crater Tycho, lat 40.9° S., long 11.5° W.
Zond 6	Nov. 1968	Unmanned flyby, first returned film	Altitude, $\geq$3,300 km.
Apollo 8	Dec. 1968	First manned orbital	Perilune, 110 km.
Apollo 10	May 1969	Manned orbital	Best perilune, 15 km.
Apollo 11	July 1969	First manned landing	Mare Tranquillitatis, lat 0.7° N., 23.4° E.
Zond 7	Aug. 1969	Unmanned flyby, returned film	Southern farside and west limb; perilune, 2,200 km(?).
Apollo 12	Nov. 1969	Manned landing	Oceanus Procellarum, lat 3.2° S., long 23.4° W.
Apollo 13	Apr. 1970	Manned flyby (aborted landing)	Southern farside and west limb.
Luna 16	Sept. 1970	First unmanned sample return	Mare Fecunditatis, lat 0.7° S., long 56.3° E.
Zond 8	Oct. 1970	Unmanned flyby, returned film	Altitude, $\geq$1,120 km.
Luna 17	Nov. 1970	Lunakhod 1, first unmanned rover	Sinus Iridum, lat 38.3° N., long 35.0° W.
Apollo 14	Feb. 1971	First manned landing in terra	Fra Mauro highlands, lat 3.7° S., long 17.5° W.
Apollo 15	July 1971	Manned landing, first long mission	Apennine-Hadley region, lat 26.1° N., long 3.7° E.
Luna 19	Oct. 1971	Unmanned orbital	Best perilune, 77 km(?).
Luna 20	Feb. 1972	Unmanned sample return	Crisium-basin rim, lat 3.5° N., long 56.5° E.
Apollo 16	Apr. 1972	Manned landing	Descartes highlands, lat 9.0° S., long 15.5° E.
Apollo 17	Dec. 1972	Last manned landing	Taurus-Littrow Valley, lat 20.2° N., long 30.8° E.
Luna 21	Jan. 1973	Lunakhod 2, unmanned rover	Mare in crater Le Monnier, lat 25.8° N., long 30.5° E.
Luna 24	Aug. 1976	Last unmanned sample return	Mare Crisium, lat 12.7° N., long 62.2° E.

SUBSURFACE

Spacecraft exploration has provided some information about the configuration of materials below the lunar surface. The uppermost layers of both the maria and the terrae consist of fragmental material called *regolith* (Shoemaker and others, 1967a, 1968). Regoliths are generally thinner than about 5 or 6 m on the maria and thicker than that on the terrae (Shoemaker and Morris, 1970; Cooper and others, 1974). They dominate the lunar scene at closeup scales (fig. 1.10) but are not evident in the telescopic and Lunar Orbiter photographs shown here, except as they affect albedo (figs. 1.1–1.9). The term "soil" is commonly used either as a synonym for regolith or in reference to its fine surficial material. Because this volume emphasizes regional relations, it does not discuss the regolith in detail.

The underlying *bedrock* of the maria is basaltic and has a density of 3.3 to 3.4 g/cm^3. Mare basalt typically extends hundreds of meters below the surface and locally reaches depths of about 5 km (see chap. 5). In contrast, the terra bedrock is feldspathic (plagioclase-rich) material with a lower density estimated at 2.90 to 3.05 g/cm^3 (Basaltic Volcanism Study Project, 1981, p. 671). Seismic data indicate that this terra material forms a crust 45 to 60 km thick in the west-central nearside (fig. 1.11; Toksöz and others, 1974; Koyama and Nakamura, 1979) and 75 km thick in part of the southeastern nearside (beneath the Apollo 16 landing site; Nakamura, 1981). Extrapolations of these measurements to other regions are based on elevation data, estimates of the crustal density, and models of isostatic compensation, all of which are subject to further refinement (Solomon, 1978; Thurbur and Solomon, 1978). Where measured, average elevations are higher, relative to the Moon's center of mass, on the farside than on the nearside (Kaula and others, 1974; Bills and Ferrari, 1977); the crust may be as thick as 120 km under some elevated terra on the farside (fig. 1.12; Bills and Ferrari, 1977). Most estimates of the mean crustal thickness fall within the range 74 ± 12 km (Kaula and others, 1974; Bills and Ferrari, 1977; Kaula, 1977; Haines and Metzger, 1980; Basaltic Volcanism Study Project, 1981, p. 671; Taylor, 1982, p. 180-182). A mean thickness of 62 km corresponds to about 10 percent of the Moon's volume, of 74 km to about 12 percent, and of 86 km to about 14 percent (radius, 1,738 km).

Little is known about lunar intracrustal structure, except that seismic velocities appear to increase at about 20 to 25 km below the surface of southern Oceanus Procellarum (Toksöz and others, 1974). This discontinuity may indicate a change in physical state (open cracks above; solid, denser material below) or in chemical composition (Todd and others, 1973; Herzberg and Baker, 1980). At least the upper few kilometers of the terra crust consists of breccia, a rock type composed of angular fragments (clasts) set in a finer-grained matrix.

Beneath the terra crust and constituting all or most of the remaining lunar volume is the ultramafic lunar mantle (fig. 1.11). Its density is close to that of mare basalt and to the mean lunar density, 3.34 g/cm^3. Seismic data suggest that the mantle is fairly uniform at least to $1,100 \pm 100$-km depth, although small seismic-velocity changes have been modeled (Goins and others, 1979). Seismic shear waves are attenuated below $1,100 \pm 100$ km. This central part of the Moon may or may not include melted zones and (or) a chemically distinct (metallic or sulfide-rich) core (Wiskerchen and Sonett, 1977; Goins and others, 1979; Taylor, 1982).

In the past, the mechanically deformable elastic lithosphere seems to have coincided with the terra crust, which may be considered the petrologic or chemical lithosphere (see chaps. 6, 8). Today, the elastic lithosphere must include much of the mantle as well.

These basic facts or assumptions about the lunar subsurface are needed as background for later discussions of lunar tectonism and petrogenesis and for perspective on the overall constitution of the Moon. This volume, however, mostly discusses the three-dimensional form of the materials in the upper few kilometers or tens of kilometers beneath the terra and mare surfaces.

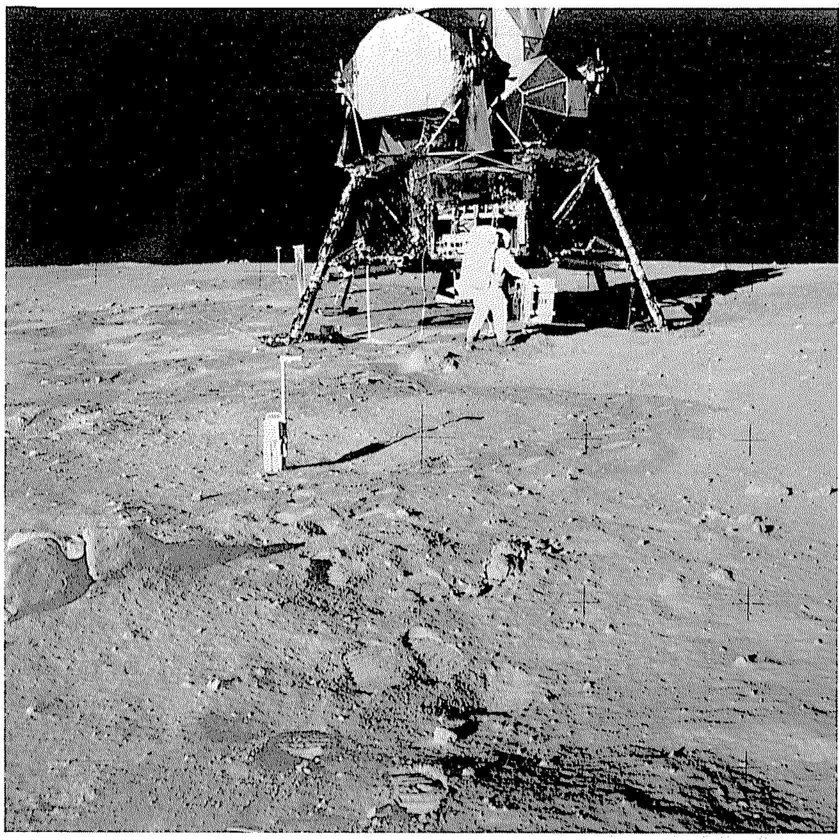

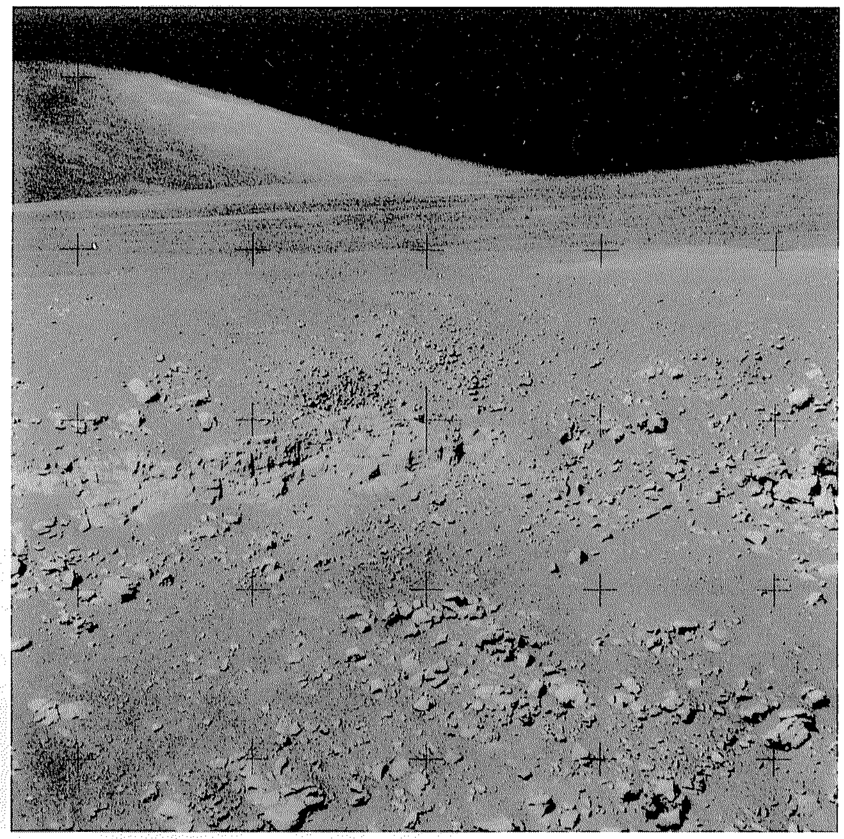

FIGURE 1.10.—Astronaut views of lunar surface.
A. Lunar Module and astronaut at Apollo 11 landing site. Regolith consists of loose, footprint-compacted material and a few rocks. Apollo 11 frame H–5931.

B. Wall of Rima Hadley (Hadley Rille) at Apollo 15 landing site, showing the only inplace outcrops of lunar strata visited by astronauts, overlain by thin regolith and loose boulders. Montes Apenninus, in distance, appear smooth because of cover of loose debris (compare rugged appearance of mountains in fig. 1.6). Apollo 15 frame H–12115.

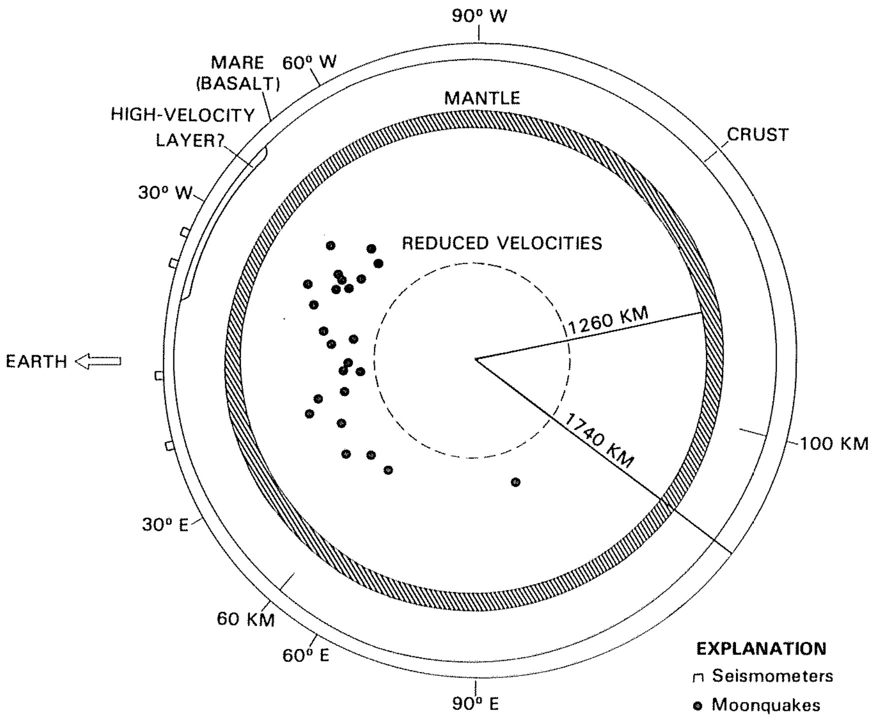

A

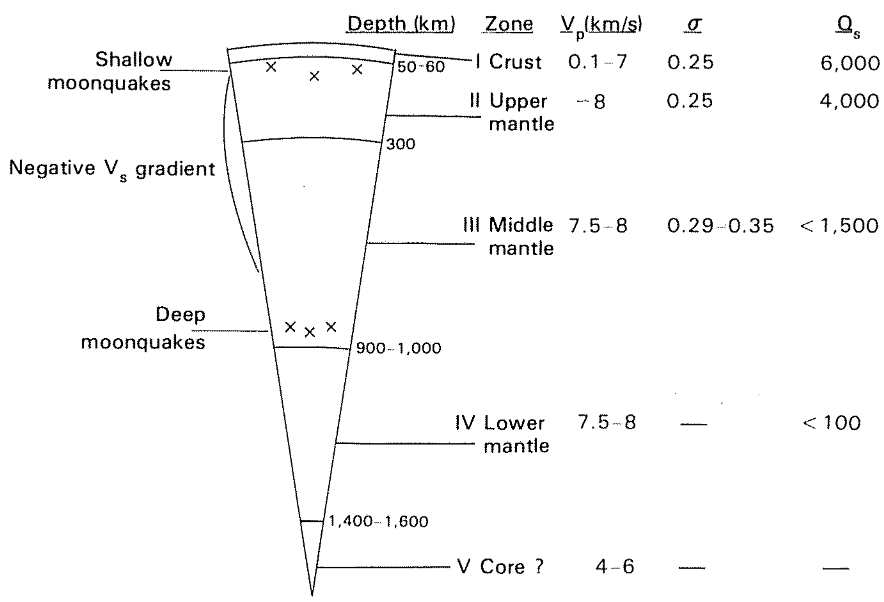

B

FIGURE 1.11.—Two interpretations of major features of lunar crust and mantle.
A. Schematic equatorial slice through entire Moon. All known endogenic moonquakes are on nearside. Crust believed to be thicker on farside than on nearside. Longitudes of Apollo seismometers are shown. From Goins and others (1979, fig. 6b).

B. Similar crustal structure but different mantle structure hypothesized by Latham and others (1978). V_p, compressional-wave velocity; V_s, shear-wave velocity; σ, Poisson's ratio; Q_s, quality factor for shear waves.

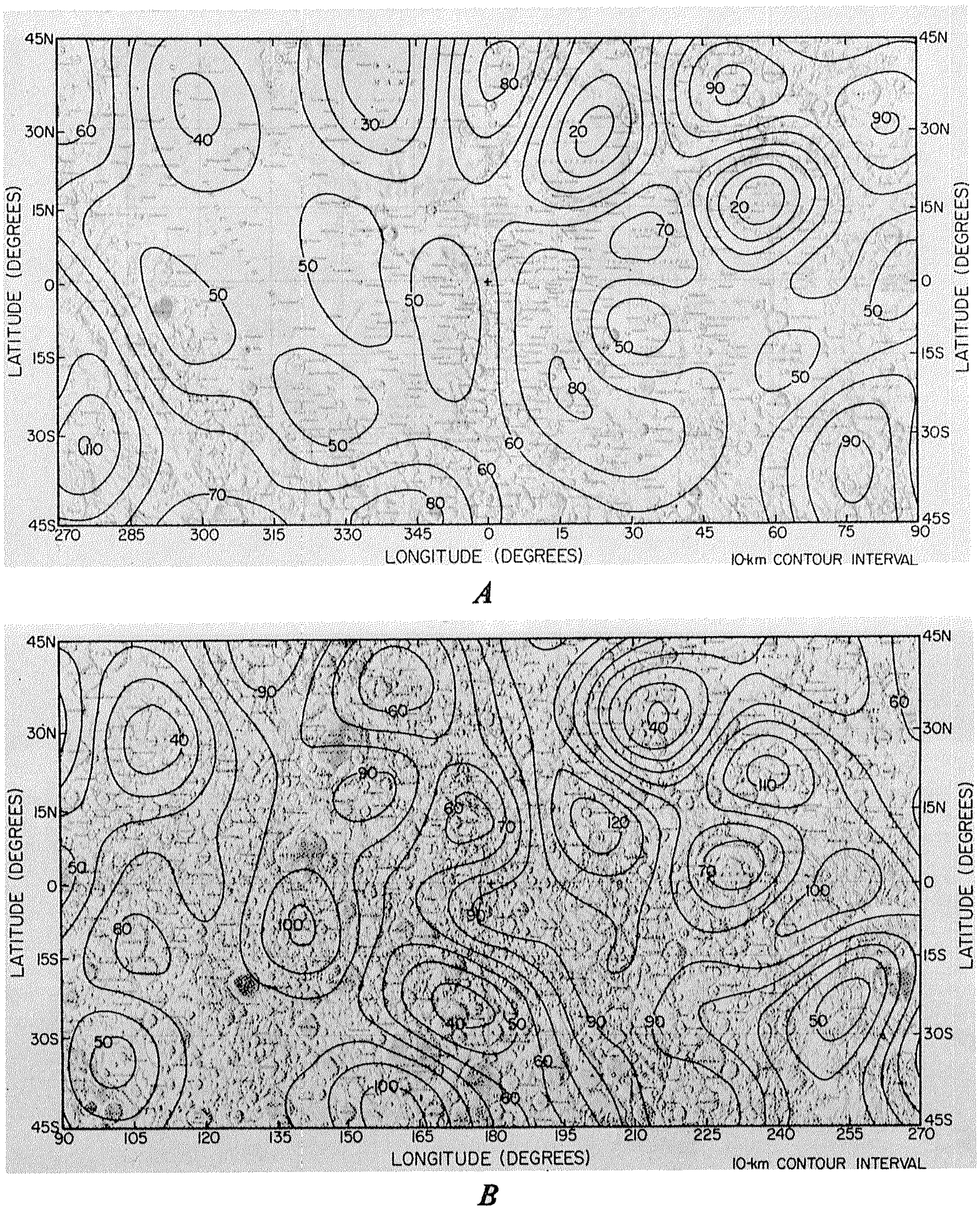

FIGURE 1.12.—Approximate crustal thicknesses (in kilometers) on nearside (*A*) and farside (*B*). From Bills and Ferrari (1977, fig. 3).